

Observer-based asynchronous self-triggered control for a dynamic positioning ship with the hysteresis input

Guoqing ZHANG^{1*}, Mingqi YAO¹, Qihe SHAN¹ & Weidong ZHANG²¹Navigation College, Dalian Maritime University, Dalian 116026, China;²Department of Automation, Shanghai Jiao Tong University, Shanghai 200240, China

Received 20 December 2021/Revised 2 March 2022/Accepted 19 April 2022/Published online 26 October 2022

Abstract This paper focuses on the asynchronous self-triggered control scheme for a dynamic positioning ship considering the hysteresis input. A novel self-triggered mechanism is designed to relax the limitation of the continuous monitoring required for the triggered condition, and the next triggered instant depends on the information at the current instant. In particular, multiple controller-thruster channels are asynchronously self-triggered; i.e., the self-triggered mechanism for each thruster is independent and noninteracting. A neural network observer is constructed to estimate the unavailable velocities for the control design. Meanwhile, unknown backlash-like hysteresis inputs are considered in this scheme through the fusion of the adaptive backstepping recursive design technique. Furthermore, the explosion of complexity existing in conventional backstepping design is avoided on the basis of the dynamic surface technique. Through the Lyapunov theory, considerable effort is made to guarantee semi-global uniform ultimate bounded stability. Finally, numerical simulations are provided to validate the feasibility of the proposed scheme.

Keywords dynamic positioning ship, self-triggered control, neural networks, hysteresis input, robust control

Citation Zhang G Q, Yao M Q, Shan Q H, et al. Observer-based asynchronous self-triggered control for a dynamic positioning ship with the hysteresis input. *Sci China Inf Sci*, 2022, 65(11): 212206, <https://doi.org/10.1007/s11432-021-3496-6>

1 Introduction

With the increasing requirements for automatic control systems in the field of ocean engineering, advanced dynamic positioning (DP) systems have aroused wide concern. These systems play a key role in oil and gas industries, such as drilling rigs, cable and pipe layers, and floating production storage and offloading units (FPSOs) [1]. In practice, the limited communication bandwidth can hardly accommodate the continuous transmission of control signals between the controller and thrusters, which can result in network congestion, network delay, and data dropout. Moreover, hysteresis characteristics are ubiquitous in the physical mechanical actuation devices, especially for a DP ship stabilized in a preset position. This condition may cause instability in the closed-loop system and even lead to the invalidation of some conventional theoretical algorithms. Therefore, the investigation of the DP control, with consideration of the limited communication bandwidth and hysteresis characteristics, requires to play more extensive attention and is meaningful in the ocean industry.

For some existing DP control schemes [2, 3], dynamic model parameters require to be precisely known. However, these parameters depend on the marine environment and its characteristics, so unknown uncertainties in the model exist. In the presence of this problem, a multitude of theoretical research has been reported in [4]. For instance, an adaptive fuzzy system was utilized to remodel unknown dynamic model parameters in [5], which would further improve the control performance of the system. With an eye to unknown model uncertainties and environmental disturbances, radial basis function neural networks

* Corresponding author (email: zgq_dlmu@163.com)

(NNs) were employed to compensate for uncertain terms, with the NN weight matrix being updated online [6]. Furthermore, the robust neural damping technique and dynamic surface control (DSC) were combined to approximate the uncertain term in model [7]. Particularly, the NN weight was compressed to reduce the computational burden; i.e., the weight was eliminated and no longer required to be updated online.

Most existing DP systems are network control systems with the merits of easy expansion, low cost, and resource sharing. However, the communication channel bandwidth is limited, which would easily lead to network congestion due to the continuous signal transmission between the controller and actuator. With this challenge, the event-triggered concept has been proposed by researchers at home and abroad [4]. In [8], an event-triggered mechanism was designed to generate non-periodic updated control input, which would reduce the signal transmission frequency. The switching event-triggered mechanism is proposed on the basis of the fixed threshold strategy and relative threshold strategy in [9]. For example, the relative threshold strategy is adopted under normal circumstances, and the fixed threshold strategy is used when the magnitude of the control signal is excessively large. Different from the conventional event-triggered control schemes [10–12], event-based parameter estimators are designed and they are event-triggered simultaneously using the controller [13]. The estimators are easy to calculate and do not need to perform real-time integration. In [14], a novel dynamic event-triggered mechanism was proposed through the fusion of the feedback domination technique. This scheme adopts the discrete-time control strategy and provides the explicit scaling gain and selection regions of the sampling period.

However, these aforementioned schemes suffered from three major problems. The first problem is unavailable velocities; i.e., only the ship position can be measured in practice engineering. Although increased measurement instruments can stimulate velocity variables to be measurable in practice, dead reckoning can only be provided by observers in the case of the sensor failure [15,16]. The second problem is the conventional event-triggered control schemes, where triggered conditions have to be continuously monitored. This task is difficult to achieve in hardware. Considering the applicability of control schemes, self-triggered strategies came into being [17–19]. The third problem is hysteresis nonlinearities in actuators. Actually, the hysteresis phenomenon is universal for actuating devices in marine practices [20]. This condition may impact systems control performance and even lead to the instability of the closed-loop system.

Motivated by the above observations, an adaptive asynchronous self-triggered DP control scheme for a fully-actuated ship is proposed; the scheme is performed by employing an NN observer, DSC, and hysteresis input with the merits of easy implementation, velocity observability, and small communication burden. Different from the traditional DP control schemes [6, 21], the physical actuation process is considered in the proposed algorithm, with the thruster pitch ratio being used as the actual control input. The main contributions of this paper can be summarized as follows.

(1) A novel asynchronous self-triggered control scheme is proposed subject to the communication bandwidth limitation. In the scheme, control signals in each thruster are designed with a self-triggered mechanism. They are independent and do not influence one another; e.g., control signals can realize asynchronous transmission in controller-thruster channels. Different from the conventional event-triggered control scheme [8,10], the self-triggered control scheme relaxes the limitation that the triggered condition requires to be continuously monitored. That is, the next triggered instant can be computed by the information at the current instant. This technique not only relieves the communication burden caused by frequently transmitting signals, but is also convenient for physical realization in practice engineering.

(2) Unavailable velocities can be estimated by the designed NN state observer. This would abolish the restrictive condition in [22,23] where all system states are available for measurement. Meanwhile, unknown backlash-like hysteresis inputs, ubiquitously existing in physical actuation devices, are considered in the proposed scheme. Hysteresis nonlinearities are compensated with the aid of the adaptive backstepping technique without constructing a hysteresis inverse. This technique is particularly convenient for stability analysis.

The remaining of this paper is organized as follows. Section 2 introduces the problem formulation and preliminaries. The observer-based asynchronous self-triggered dynamic positioning control design is presented in Section 3. Section 4 analyzes the stability and robustness of the closed-loop system. In Section 5, numerical simulations are provided to verify the effectiveness of the proposed scheme. Section 6 concludes the whole paper.

2 Problem formulation and preliminaries

Throughout the paper, $|\cdot|$ implies the absolute operator for the scalar element. $\|\cdot\|$ indicates the Euclidean norm of a vector and $\|\cdot\|_F$ denotes the Frobenius norm. The matrix $\|\mathbf{A}\|_F^2 = \text{tr}\{\mathbf{A}^T \mathbf{A}\} = \sum_{i=1}^m \sum_{j=1}^n a_{i,j}^2$, where $\mathbf{A} = [a_{i,j}] \in \mathbb{R}^{m \times n}$ is a matrix. $\hat{(\cdot)}$ indicates the estimate of (\cdot) and the estimation error $\tilde{(\cdot)} = \hat{(\cdot)} - (\cdot)$; sgn is the sign function; “ \cdot .” implies the element-by-element multiplication; $\text{diag}\{c_1, c_2, \dots, c_n\}$ denotes the main diagonal matrix, where c_1, c_2, \dots, c_n describe the diagonal elements.

2.1 Problem formulation

Referring to the seakeeping and maneuvering theory [24], the three-degree of freedom (3-DOF) nonlinear mathematical model of the DP vehicle could be described as

$$\dot{\boldsymbol{\eta}} = \mathbf{R}(\psi) \mathbf{v}, \quad \mathbf{M}\dot{\mathbf{v}} + \mathbf{D}_l \mathbf{v} + \mathbf{D}_n(\mathbf{v}) = \boldsymbol{\tau} + \mathbf{d}_w, \quad (1)$$

$$\mathbf{R}(\psi) = \begin{bmatrix} \cos \psi & -\sin \psi & 0 \\ \sin \psi & \cos \psi & 0 \\ 0 & 0 & 1 \end{bmatrix}, \quad \mathbf{M} = \begin{bmatrix} m - X_{\dot{u}} & 0 & 0 \\ 0 & m - Y_{\dot{v}} & mx_G - Y_{\dot{r}} \\ 0 & mx_G - Y_{\dot{r}} & I_z - N_{\dot{r}} \end{bmatrix}, \quad (2)$$

$$\mathbf{D}_l = \begin{bmatrix} -X_u & 0 & 0 \\ 0 & -Y_v & -Y_r \\ 0 & -N_v & -N_r \end{bmatrix}, \quad \mathbf{D}_n(\mathbf{v}) = \begin{bmatrix} -X_{|u|u} |u| u + Y_{\dot{v}} v |r| + Y_{\dot{r}} r r \\ -X_{\dot{u}} u r - Y_{|v|v} |v| v - Y_{|v|r} |v| r \\ (X_{\dot{u}} - Y_{\dot{v}}) u v - Y_{\dot{r}} u r - N_{|v|v} |v| v - N_{|v|r} |v| r \end{bmatrix}, \quad (3)$$

$$\boldsymbol{\tau} = \mathbf{T}(\beta) \boldsymbol{\kappa}(\mathbf{n}) \mathbf{u}_p. \quad (4)$$

In (1), $\boldsymbol{\eta} = [x, y, \psi]^T \in \mathbb{R}^3$ indicates the ship attitude vector with (x, y) and ψ being the position coordinate and the heading angle, respectively. $\mathbf{v} = [u, v, r]^T \in \mathbb{R}^3$ denotes the velocity vector, where u, v, r are velocities in the surge, sway, and yaw, respectively. $\mathbf{R}(\psi)$ implies the velocity rotation matrix with $\mathbf{R}^{-1}(\psi) = \mathbf{R}^T(\psi)$, $\|\mathbf{R}(\psi)\| = 1$. \mathbf{M} is the mass matrix with the detailed expressions being given in (2), where I_z, m are the moment of inertia and ship’s mass, x_G denotes the longitudinal coordinate of the ship’s center of gravity in body-fixed frame, $Y_{\dot{v}}, Y_{\dot{r}}$ are added mass, $N_{\dot{r}}$ indicates added moment of inertia. $\mathbf{D}_l, \mathbf{D}_n(\mathbf{v})$ are the linear and nonlinear hydrodynamic term, respectively, which are shown in (3). Around \mathbf{D}_l and $\mathbf{D}_n(\mathbf{v})$, $X_u, X_{|u|u}, Y_{|v|v}, \dots$ are all the hydrodynamic force derivatives.

$\boldsymbol{\tau} = [\tau_u, \tau_v, \tau_r]^T \in \mathbb{R}^3$ indicates the control input vector, where τ_u, τ_v are the control forces in the surge and sway, and τ_r is the control moment in the yaw. $\mathbf{d}_w = [d_{wu}, d_{wv}, d_{wr}]^T \in \mathbb{R}^3$ implies the marine environmental disturbance vector, where d_{wu}, d_{wv} indicate the disturbance forces in the surge and sway, and d_{wr} denotes the disturbance moment in the yaw. $\mathbf{T}(\beta) \in \mathbb{R}^{3 \times q}$ is the thrust configuration matrix depending on the physical location of thrusters, where q indicates the number of equivalent thrusters and β denotes the bearing angle in the rotatable thruster. $\boldsymbol{\kappa}(\mathbf{n}) = \text{diag}\{\kappa_1(n_1), \kappa_2(n_2), \dots, \kappa_q(n_q)\} \in \mathbb{R}^{q \times q}$ is unknown force coefficient matrix associated with the propeller speed n_i , where $i = 1, 2, \dots, q$. $\mathbf{u}_p = [u_{p1}, u_{p2}, \dots, u_{pq}]^T$ is the control law of the system considering the hysteresis nonlinearity with $u_{pi} = |p_{hi}| p_{hi}$, where p_{hi} indicates hysteresis input. Then the unknown backlash-like hysteresis phenomenon can be described as

$$\frac{du_{pi}}{dt} = \xi_i \left| \frac{dv_{pi}}{dt} \right| (k_{pi} v_{pi} - u_{pi}) + \zeta_i \frac{dv_{pi}}{dt}, \quad (5)$$

where $v_{pi} = |p_{si}| p_{si}$ with p_{si} being the self-triggered controllable input (pitch ratio) for the i th thruster, ξ_i, k_{pi}, ζ_i indicate the unknown constant parameters.

Referring to [25], the solution of (5) can be expressed as

$$\mathbf{u}_p = \mathbf{k}_p \mathbf{v}_p + \mathbf{l}(\mathbf{v}_p), \quad (6)$$

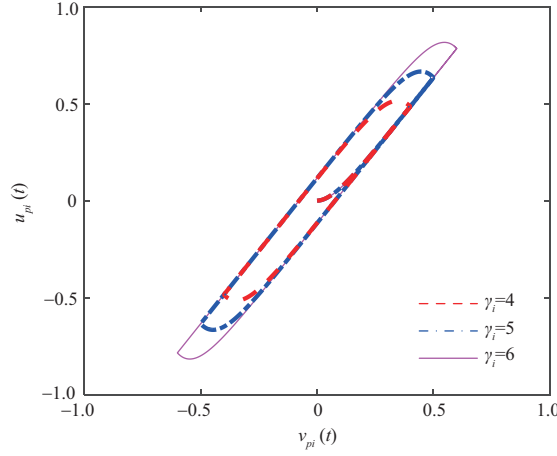


Figure 1 (Color online) Backlash-like hysteresis input curves.

$$\begin{aligned}
 l_i(v_{pi}) = & [u_{pi}(0) - k_{pi}v_{pi}(0)] e^{-\xi_i(v_{pi}-v_{pi}(0))\text{sgn}\dot{v}_{pi}} \\
 & + e^{-\xi_i v_{pi}\text{sgn}\dot{v}_{pi}} \int_{v_{pi}(0)}^{v_{pi}} [\zeta_i - k_{pi}] e^{\xi_i \varpi (\text{sgn}\dot{v}_{pi})} d\varpi,
 \end{aligned} \quad (7)$$

where $\mathbf{u}_p = [u_{p1}, u_{p2}, \dots, u_{pq}]^T$, $\mathbf{k}_p = \text{diag}[k_{p1}, k_{p2}, \dots, k_{pq}]$, $\mathbf{l}(\mathbf{v}_p) = [l_1(v_{p1}), l_2(v_{p2}), \dots, l_q(v_{pq})]^T$. $u_{pi}(0)$ and $v_{pi}(0)$ denote the initial conditions of u_{pi} and v_{pi} , respectively. Actually, $l_i(v_{pi})$ is bounded, and satisfies $|l_i(v_{pi})| \leq \bar{l}_i$ with $\bar{l}_i > 0$ being unknown constant [25]. The backlash-like hysteresis characteristics are shown in Figure 1 with $v_{pi} = \gamma_i \sin(2.3t)$, $\xi_i = 12$, $\zeta_i = 0.105$, $k_{pi} = 1.5$, $u_{pi}(0) = 0$.

Assumption 1. The mass matrix \mathbf{M} is positive-definite and invertible. Actually, the marine surface ship usually satisfies the port-starboard symmetry and fore-aft approximate symmetry in practice. Thus, this condition is satisfied automatically.

Assumption 2. The environment disturbance term \mathbf{d}_w is bounded vector; i.e., there exists an unknown positive constant vector $\bar{\mathbf{d}}_w = [\bar{d}_{wu}, \bar{d}_{wv}, \bar{d}_{wr}]^T$ with $|d_{wu}| \leq \bar{d}_{wu}$, $|d_{wv}| \leq \bar{d}_{wv}$, $|d_{wr}| \leq \bar{d}_{wr}$.

Assumption 3. The force coefficient of thruster is a constant, e.g., $0 < \underline{\kappa}_i \leq \kappa_i(n_i) \leq \bar{\kappa}_i$, $i = 1, 2, \dots, q$, where $\underline{\kappa}_i$ and $\bar{\kappa}_i$ are unknown constants. This condition is satisfied automatically in practical engineering because the thruster's energy is certainly finite.

Remark 1. In practical engineering, the fully-actuated ship is usually equipped with the rotatable thrusters to improve the control performance. However, this presents a serious challenge to control design; i.e., there exists a bearing angle β in the thrust configuration matrix. Thus, the rotatable thruster can be extended as two forces. Taking a marine surface ship with two main propellers and one rotatable thruster as an example, the extending operation is shown as

$$\begin{aligned}
 \boldsymbol{\tau} &= \underbrace{\begin{bmatrix} 1 & 1 & \cos(\beta_3) \\ 0 & 0 & \sin(\beta_3) \\ l_{y1} & -l_{y2} & l_{x3} \sin(\beta_3) \end{bmatrix}}_{\text{The actual matrix } \mathbf{T}(\beta)} \begin{bmatrix} \kappa_1 & 0 & 0 \\ 0 & \kappa_2 & 0 \\ 0 & 0 & \kappa_3 \end{bmatrix} \begin{bmatrix} u_1 \\ u_2 \\ u_3 \end{bmatrix} \\
 &= \underbrace{\begin{bmatrix} 1 & 1 & 1 & 0 \\ 0 & 0 & 0 & 1 \\ l_{y1} & -l_{y2} & 0 & l_{x3} \end{bmatrix}}_{\text{The extended matrix}} \begin{bmatrix} \kappa_1 & 0 & 0 & 0 \\ 0 & \kappa_2 & 0 & 0 \\ 0 & 0 & \kappa_3 & 0 \\ 0 & 0 & 0 & \kappa_3 \end{bmatrix} \begin{bmatrix} u_1 \\ u_2 \\ u_{3x} \\ u_{3y} \end{bmatrix}.
 \end{aligned} \quad (8)$$

Furthermore, the equivalent control inputs $u_{3x} = u_3 \cos(\beta_3)$, $u_{3y} = u_3 \sin(\beta_3)$ can be derived by employing the logical coordinate transformation (9).

$$u_3 = |p_3| p_3 = \sqrt{u_{3x}^2 + u_{3y}^2}, \quad \beta_3 = \arctan(u_{3x}, u_{3y}). \quad (9)$$

2.2 RBF NNs

In this paper, the RBF NNs are employed to approximate the model dynamic uncertainties with the advantage of excellent function approximation capability.

Lemma 1 ([26,27]). For any given continuous function $f(\mathbf{x})$ with $f(\mathbf{0}) = 0$, $f(\mathbf{x})$ can be described as (10) on the basis of the radical basic function (RBF) NN approximation and the continuous function separation techniques.

$$f(\mathbf{x}) = \mathbf{W}^T \mathbf{S}(\mathbf{x}) + \varepsilon(\mathbf{x}), \quad \forall \mathbf{x} \in \Omega_{\mathbf{x}}. \quad (10)$$

The input vector \mathbf{x} is defined in a compact set $\mathbb{B}_{\mathbf{x}}$ with $\mathbb{B}_{\mathbf{x}} \in \mathbb{R}^n$. $\mathbf{W} = [w_1, w_2, \dots, w_l]^T \in \mathbb{R}^l$ is the weight vector, $\varepsilon(\mathbf{x})$ denotes the approximation error with the unknown upper bound $\bar{\varepsilon}$. $\mathbf{S}(\mathbf{x}) = [s_1(\mathbf{x}), s_2(\mathbf{x}), \dots, s_l(\mathbf{x})]^T$ is an RBF vector, which is chosen as Gaussian function:

$$s_j(\mathbf{x}) = \frac{1}{\sqrt{2\pi}\zeta_j} \exp\left(-\frac{(\mathbf{x} - \boldsymbol{\mu}_j)^T (\mathbf{x} - \boldsymbol{\mu}_j)}{2\zeta_j^2}\right), \quad (11)$$

where $j = 1, 2, \dots, l$, $\boldsymbol{\mu}_j = [\mu_{j1}, \mu_{j2}, \dots, \mu_{jm}]$ is the center of the receptive field, ζ_j indicates the width of the Gaussian function, l implies the node number of NN, m denotes the dimension number of the state vector \mathbf{x} . For all $\mathbf{x} \in \mathbb{B}_{\mathbf{x}}$, the target weight vector \mathbf{W} and the activation function $\mathbf{S}(\mathbf{x})$ are upper bounded, e.g., $\|\mathbf{W}\| \leq \mathbf{W}_M$, $\|\mathbf{S}(\mathbf{x})\| \leq \mathbf{S}_M$, where $\mathbf{W}_M, \mathbf{S}_M$ are unknown positive constants.

Assumption 4 ([28,29]). The activation function $\mathbf{S}(\mathbf{x})$ satisfies the Lipschitz continuity condition, such that $\|\mathbf{S}(\hat{\mathbf{x}}) - \mathbf{S}(\mathbf{x})\| \leq L_x \|\hat{\mathbf{x}} - \mathbf{x}\|$ with L_x being a known constant.

3 Observer-based asynchronous self-triggered dynamic positioning control design

In this section, the NN state observer is constructed to estimate the unavailable velocity in Subsection 3.1, and the asynchronous self-triggered dynamic positioning control design procedure is shown in Subsection 3.2, which includes two steps for the kinematic and kinetic parts.

3.1 NN observer

The state observer is designed as

$$\begin{cases} \dot{\hat{\boldsymbol{\eta}}} = \mathbf{R}(\psi) \hat{\mathbf{v}} - \mathbf{C} \hat{\boldsymbol{\eta}}, \\ \mathbf{M} \dot{\hat{\mathbf{v}}} = -\hat{\mathbf{W}}_v^T \mathbf{S}_v(\hat{\mathbf{v}}) + \boldsymbol{\tau} - \mathbf{Q} \hat{\mathbf{v}} - \mathbf{R}^T(\psi) \hat{\boldsymbol{\eta}} \end{cases} \quad (12)$$

by employing the NN approximator, where $\mathbf{C} = \text{diag}\{C_u, C_v, C_r\}$ and $\mathbf{Q} = \text{diag}\{Q_u, Q_v, Q_r\}$ are all design constant matrices, $\hat{\mathbf{W}}_v = \text{diag}\{\hat{\mathbf{W}}_u, \hat{\mathbf{W}}_v, \hat{\mathbf{W}}_r\} \in \mathbb{R}^{3l \times 3}$, $\mathbf{S}_v(\hat{\mathbf{v}}) = [\mathbf{S}_u(\hat{\mathbf{v}}), \mathbf{S}_v(\hat{\mathbf{v}}), \mathbf{S}_r(\hat{\mathbf{v}})]^T \in \mathbb{R}^{3l}$.

By fusion of Lemma 1, the RBF NNs are employed to approximate the unknown uncertainty term $\mathbf{D}_l \mathbf{v} + \mathbf{D}_n(\mathbf{v})$ in the closed-loop system (1),

$$\mathbf{f}_{NN}(\mathbf{v}) = \mathbf{D}_l \mathbf{v} + \mathbf{D}_n(\mathbf{v}) = \mathbf{W}_v^T \mathbf{S}_v(\mathbf{v}) + \boldsymbol{\varepsilon}_v, \quad (13)$$

where $\mathbf{W}_v \in \mathbb{R}^{3l \times 3}$, $\mathbf{S}_v(\mathbf{v}) \in \mathbb{R}^{3l}$, $\boldsymbol{\varepsilon}_v = [\varepsilon_u, \varepsilon_v, \varepsilon_r]^T \in \mathbb{R}^3$, the upper bound vector of $\boldsymbol{\varepsilon}_v$ is $\bar{\boldsymbol{\varepsilon}}_v$.

Then the observer dynamic error can be described as

$$\begin{cases} \dot{\tilde{\boldsymbol{\eta}}} = \mathbf{R}(\psi) \tilde{\mathbf{v}} - \mathbf{C} \tilde{\boldsymbol{\eta}}, \\ \mathbf{M} \dot{\tilde{\mathbf{v}}} = -\tilde{\mathbf{W}}_v^T \mathbf{S}_v(\hat{\mathbf{v}}) - \mathbf{R}^T(\psi) \tilde{\boldsymbol{\eta}} - \mathbf{Q} \tilde{\mathbf{v}} + \boldsymbol{\varepsilon}_v - \mathbf{d}_w - \mathbf{W}_v^T (\mathbf{S}_v(\hat{\mathbf{v}}) - \mathbf{S}_v(\mathbf{v})). \end{cases} \quad (14)$$

3.2 Control design

Step 1. Define the attitude error vector $\boldsymbol{\eta}_e = \boldsymbol{\eta}_d - \boldsymbol{\eta}$ with $\boldsymbol{\eta}_d \in \mathbb{R}^3$ being the constant vector. Then one can obtain

$$\dot{\boldsymbol{\eta}}_e = \dot{\boldsymbol{\eta}}_d - \mathbf{R}(\psi) \mathbf{v} = -\mathbf{R}(\psi) \hat{\mathbf{v}} + \mathbf{R}(\psi) \tilde{\mathbf{v}}. \quad (15)$$

The virtual control law α_1 could be chosen as

$$\alpha_1 = \mathbf{R}^{-1}(\psi) \mathbf{k}_\eta \eta_e \tag{16}$$

for the velocity variable $\hat{\mathbf{v}}$ on account of (15), where \mathbf{k}_η is the strictly positive design parameter with the form of diagonal matrix. Note that, the DSC technique is employed to eliminate this restriction that the differential expression of the virtual control law α_1 is extremely complicated and difficult to be obtained,

$$\chi_1 \dot{\beta}_1 + \beta_1 = \alpha_1, \quad \beta_1(0) = \alpha_1(0), \tag{17}$$

where $\chi_1 = \text{diag}\{\chi_u, \chi_v, \chi_r\}$ indicates the time constant matrix, and β_1 presents the reference signal for the velocity vector $\hat{\mathbf{v}}$. Then one defines the filter error vector $\mathbf{q}_e = [q_u, q_v, q_r]^T = \alpha_1 - \beta_1$, $\mathbf{v}_e = \beta_1 - \hat{\mathbf{v}}$, the derivative of $\dot{\mathbf{q}}_e$ can be derived as

$$\dot{\mathbf{q}}_e = -\dot{\beta}_1 + \dot{\alpha}_1 = -\chi_1^{-1} \mathbf{q}_e + \mathbf{B}_v(\eta_e, \dot{\eta}_e, \psi, \dot{\psi}), \tag{18}$$

where $\mathbf{B}_v(\cdot) = [B_u(\cdot), B_v(\cdot), B_r(\cdot)]^T$ is a vector with its elements being continuous functions. Then the attitude dynamic error $\dot{\eta}_e$ could be described as

$$\dot{\eta}_e = -\mathbf{k}_\eta \eta_e + \mathbf{R}(\psi) \mathbf{v}_e + \mathbf{R}(\psi) \mathbf{q}_e + \mathbf{R}(\psi) \tilde{\mathbf{v}}. \tag{19}$$

Step 2. By the fusion of Lemma 1, (1), and (6), one can obtain

$$\dot{\mathbf{v}}_e = \mathbf{M}^{-1} \left[\mathbf{M} \dot{\beta}_1 + \hat{\mathbf{W}}_v^T \mathbf{S}_v(\hat{\mathbf{v}}) - \mathbf{T}(\beta) \boldsymbol{\kappa}(\mathbf{n}) \mathbf{k}_p \mathbf{v}_p - \mathbf{T}(\beta) \boldsymbol{\kappa}(\mathbf{n}) \mathbf{l}(\mathbf{v}_p) + \mathbf{R}^T(\psi) \tilde{\boldsymbol{\eta}} + \mathbf{Q} \tilde{\mathbf{v}} \right]. \tag{20}$$

The immediate control law α_2 is designed as

$$\alpha_2 = \mathbf{k}_v \mathbf{v}_e + \dot{\beta}_1 + \hat{\mathbf{W}}_v^T \mathbf{S}_v(\hat{\mathbf{v}}) + \mathbf{R}^T(\psi) \eta_e \tag{21}$$

for the desired thrust term $\mathbf{T}(\beta) \boldsymbol{\kappa}(\mathbf{n}) \mathbf{v}_p$.

The NN weight update law could be derived as

$$\dot{\hat{\mathbf{W}}}_m = \boldsymbol{\Gamma}_{wm} \left[\mathbf{S}_m(\hat{\mathbf{v}}) m_e - \sigma_{wm} (\hat{\mathbf{W}}_m - \hat{\mathbf{W}}_m(0)) \right] \tag{22}$$

with $m = u, v, r$, where $\boldsymbol{\Gamma}_{wm} \in \mathbb{R}^{l \times l}$ denotes the positive design matrix, σ_{wm} is the positive constant parameter.

The self-triggered mechanism is designed as follows for the i th thruster:

$$v_{pi}(t) = \omega_{pi}(t_k), \quad \forall t \in [t_k, t_{k+1}), \tag{23}$$

$$t_{k+1} = t_k + \frac{\delta_i |v_{pi}(t)| + \epsilon_i}{\max\{D, |\dot{\omega}_{pi}(t_k)|\}}, \tag{24}$$

where ω_{pi} indicates the actual control law for the i th actuator's actual control input, $t_k \in \mathbb{Z}^+$ indicates the triggered instants, $0 < \delta_i < 1$, $\epsilon_i > 0$, $D > 0$ are all the positive design parameters. At triggered instants t_k , the control signal $v_{pi}(t_k)$ would be updated and transmitted to the i th thruster. And the control signal $v_{pi}(t)$ would be held during the time $t \in [t_k, t_{k+1})$. The next triggered instant t_{k+1} is able to be computed on the basis of control signal $v_{pi}(t_k)$ in the last triggered instant.

Remark 2. In the practical engineering, the thruster's energy is certainly finite. Thus, the control signal $v_{pi}(t)$ is guaranteed to be bounded with $\omega_{pi}(t)$ being bounded, and the detailed expression for $\boldsymbol{\omega}_p = [\omega_{p1}, \omega_{p2}, \dots, \omega_{pq}]^T$ has been given in (32). The boundedness of the control signal $v_{pi}(t)$ could guarantee that the triggered interval time $\Delta t = t_{k+1} - t_k$ is not infinitely great. Then the positive design parameters δ_i , ϵ_i , and D are employed to guarantee that the term $(\delta_i |v_{pi}(t)| + \epsilon_i) / (\max\{D, |\dot{\omega}_{pi}(t_k)|\})$ is strictly positive variable. Obviously, the lower bound of triggered interval time $\Delta t > 0$ could be guaranteed by incorporating (23) and (24). Therefore, the Zeno behavior is avoided successfully; e.g., there exist no triggered instants to be accumulated in this proposed algorithm.

From the above self-triggered rule, $|\omega_{pi}(t) - v_{pi}(t)| \leq \delta_i |v_{pi}(t)| + \epsilon_i$ is held during all the time. Then the following two cases are discussed.

Case 1: $v_{pi}(t) \geq 0$. Under this case, $-\delta_i v_{pi}(t) - \epsilon_i \leq \omega_{pi}(t) - v_{pi}(t) \leq \delta_i v_{pi}(t) + \epsilon_i$. Thus, one has

$$\omega_{pi}(t) - v_{pi}(t) = \rho_i(t) (\delta_i v_{pi}(t) + \epsilon_i) \tag{25}$$

with $|\rho_i(t)| \leq 1$.

Case 2: $v_{pi}(t) < 0$. Under this case, $\delta_i v_{pi}(t) - \epsilon_i \leq \omega_{pi}(t) - v_{pi}(t) \leq -\delta_i v_{pi}(t) + \epsilon_i$. Then it yields

$$\omega_{pi}(t) - v_{pi}(t) = \rho_i(t) (\delta_i v_{pi}(t) - \epsilon_i). \tag{26}$$

Combining the above two cases, one can obtain

$$\omega_{pi}(t) - v_{pi}(t) = \rho_{i1}(t) \delta_i v_{pi}(t) + \rho_{i2}(t) \epsilon_i \tag{27}$$

with $\rho_{i1}(t)$ and $\rho_{i2}(t)$ satisfying

$$\begin{cases} \rho_{i1}(t) = \rho_{i2}(t) = \rho_i(t), & v_{pi}(t) \geq 0, \\ \rho_{i1}(t) = \rho_i(t), \quad \rho_{i2}(t) = -\rho_i(t), & v_{pi}(t) < 0. \end{cases} \tag{28}$$

Summarizing above the two cases, one has

$$v_{pi}(t) = \frac{\omega_{pi}}{1 + \rho_{i1}(t) \delta_i} - \frac{\rho_{i2} \epsilon_i}{1 + \rho_{i1}(t) \delta_i}. \tag{29}$$

Thus, Eq. (20) could be rewritten as

$$\begin{aligned} \dot{v}_e = M^{-1} & \left[M \dot{\beta}_1 + \hat{W}_v^T S_v(\dot{v}) - T(\beta) \kappa(n) k_p A \omega_p + Q \ddot{v} + T(\beta) \kappa(n) k_p A B \epsilon \right. \\ & \left. - T(\beta) \kappa(n) l(v_p) + R^T(\psi) \tilde{\eta} \right], \end{aligned} \tag{30}$$

where $A = \text{diag}\{1/(1 + \rho_{11}(t) \delta_1), 1/(1 + \rho_{21}(t) \delta_2), \dots, 1/(1 + \rho_{q1}(t) \delta_q)\}$, $B = \text{diag}\{\rho_{12}, \rho_{22}, \dots, \rho_{q2}\}$, $\epsilon = [\epsilon_1, \epsilon_2, \dots, \epsilon_q]^T$, $\omega_p = [\omega_{p1}, \omega_{p2}, \dots, \omega_{pq}]^T$ is the actual control law matrix for actual control input matrix $p = [p_1, p_2, \dots, p_q]^T$.

In the marine practice, the unknown term $g_{pi} = \kappa(n_i) k_{pi} / (1 + \rho_{i1}(t) \delta_i)$ may give rise to the system gain uncertainty with $g_p = \text{diag}\{g_{p1}, g_{p2}, \dots, g_{pq}\}$. To sure this term, one employs $\hat{\lambda}_i$ to estimate the $1/g_{pi}$. The potential singularity phenomenon could be eliminated by the special property and structure of $\hat{\lambda}_i$. The actual control law matrix for actual control input matrix p :

$$p = \text{sgn}(\omega_p) \cdot * \sqrt{|\omega_p|} \tag{31}$$

can be designed as

$$\omega_p = \text{diag} \left\{ \hat{\lambda}_1, \hat{\lambda}_2, \dots, \hat{\lambda}_q \right\} T^\dagger(\beta) \alpha_2, \tag{32}$$

where $T^\dagger(\beta)$ indicates the pseudo inverse of $T(\beta)$.

Then the adaptive parameters $\hat{\lambda}_i$ could be derived as

$$\dot{\hat{\lambda}}_i = \Gamma_i \left[\sum_{m=u, v, r} \sum_{n=u, v, r} T_{in}^\dagger(\beta) T_{mi}(\beta) m_e \alpha_{2n} - \sigma_i (\hat{\lambda}_i - \hat{\lambda}_i(0)) \right], \tag{33}$$

where $T_{in}^\dagger(\beta)$ denotes the element in the i th row and n th column of $T^\dagger(\beta)$, Γ_i, σ_i are the positive design parameters. It is worth mentioning that the term $\sigma_i (\hat{\lambda}_i - \hat{\lambda}_i(0))$ is able to protect the adaptive parameters $\hat{\lambda}_i$ from the drifting divergence.

4 Stability analysis

In this section, the stability analysis of the closed-loop system is presented by fusion of the assessment of the dynamic errors.

Theorem 1. Under Assumptions 1–3, the initial condition $\eta_e(0)^T \eta_e(0) + v_e(0)^T v_e(0) + q_e(0)^T q_e(0) + \sum_{m=u,v,r} \tilde{W}_m(0)^T \tilde{W}_m(0) + \sum_{i=1}^q \tilde{\lambda}_i^2(0) \leq \Delta_2$ is satisfied with any $\Delta_2 > 0$. The closed-loop system including the ship model (1), control laws (16) and (21), weight update law (22), and adaptive parameters (33) is stable. All the signals are semi-global uniformly ultimately bounded (SGUUB) by tuning the parameters $k_\eta, k_v, \Gamma_{wm}, \Gamma_i, \sigma_{wm}, \sigma_i, \delta_i, \epsilon_i, D$ appropriately.

Proof. The Lyapunov function candidate is constructed as

$$\begin{aligned} V = & \frac{1}{2} \tilde{\eta}^T \tilde{\eta} + \frac{1}{2} \tilde{v}^T M \tilde{v} + \frac{1}{2} \eta_e^T \eta_e + \frac{1}{2} v_e^T M v_e + \frac{1}{2} q_e^T q_e \\ & + \frac{1}{2} \sum_{m=u,v,r} \tilde{W}_m^T \Gamma_{wm}^{-1} \tilde{W}_m + \frac{1}{2} \sum_{i=1}^q \frac{g_{pi} \tilde{\lambda}_i^2}{\Gamma_i}. \end{aligned} \quad (34)$$

Then, the derivative of V can be derived as

$$\begin{aligned} \dot{V} = & \tilde{\eta}^T \dot{\tilde{\eta}} + \tilde{v}^T M \dot{\tilde{v}} + \eta_e^T \dot{\eta}_e + v_e^T M \dot{v}_e + q_e^T \dot{q}_e + \sum_{m=u,v,r} \tilde{W}_m^T \Gamma_{wm}^{-1} \dot{\tilde{W}}_m + \sum_{i=1}^q \frac{g_{pi}}{\Gamma_i} \tilde{\lambda}_i \dot{\tilde{\lambda}}_i \\ = & \tilde{\eta}^T (R(\psi) \tilde{v} - C \tilde{\eta}) + \tilde{v}^T \left(-\tilde{W}_v^T S_v(\hat{v}) - R^T(\psi) \tilde{\eta} - Q \tilde{v} - W_v^T (S_v(\hat{v}) - S_v(v)) \right. \\ & \left. + \varepsilon_v - d_w \right) + \eta_e^T (-k_\eta \eta_e + R(\psi) v_e + R(\psi) q_e + R(\psi) \tilde{v}) + v_e^T \left[M \dot{\beta}_1 + \hat{W}_v^T S_v(\hat{v}) \right. \\ & \left. - T(\beta) \kappa(n) k_p A \omega_p + Q \tilde{v} + T(\beta) \kappa(n) k_p A B \epsilon - T(\beta) \kappa(n) l(v_p) + R^T(\psi) \tilde{\eta} \right] \\ & + q_e^T (-\chi_1^{-1} q_e + B_v(\eta_e, \dot{\eta}_e, \psi, r)) + \sum_{m=u,v,r} \tilde{W}_m^T \dot{\tilde{W}}_m + \sum_{i=1}^q g_{pi} \tilde{\lambda}_i \dot{\tilde{\lambda}}_i. \end{aligned} \quad (35)$$

In the practical engineering, DP ship usually has to navigate to the area near the predetermined desired position, after that the ship automatically performs the dynamic positioning task. Then the variables x_e, y_e, ψ_e, ψ can be guaranteed to be bounded in a compact. Actually, the asynchronous self-triggered DP control scheme is able to guarantee that the above precondition is satisfied automatically. Therefore, the conclusion can be obtained that $\Pi := \{(x_e, \dot{x}_e, y_e, \dot{y}_e, \psi_e, \dot{\psi}_e, \psi, \dot{\psi})\}$ is compact in \mathbb{R}^8 , and there exist positive constants $\bar{B}_u, \bar{B}_v, \bar{B}_r$, such that $|B_u(\cdot)| \leq \bar{B}_u, |B_v(\cdot)| \leq \bar{B}_v, |B_r(\cdot)| \leq \bar{B}_r$.

Using Young's inequality, one can obtain the following with I being the identity matrix:

$$\begin{aligned} -\tilde{v}^T \tilde{W}_v^T S_v(\hat{v}) & \leq \frac{1}{2} \tilde{v}^T \tilde{v} + \frac{1}{2} \sum_{m=u,v,r} \tilde{W}_m^T \tilde{W}_m, \\ \hat{v}_e^T \tilde{W}_v^T S_v(\hat{v}) & \leq \frac{1}{2} \hat{v}_e^T \hat{v}_e + \frac{1}{2} \sum_{m=u,v,r} \tilde{W}_m^T \tilde{W}_m, \\ \tilde{v}^T \varepsilon_v & \leq \frac{1}{4} \tilde{v}^T \tilde{v} + \bar{\varepsilon}_v^T \bar{\varepsilon}_v, \\ -\tilde{v}^T d_w & \leq \frac{1}{4} \tilde{v}^T \tilde{v} + \bar{d}_w^T \bar{d}_w, \\ v_e^T (M - I) \dot{\beta}_1 & = v_e^T (M - I) \chi_1^{-1} q_e \\ & \leq \|(M - I) \chi_1^{-1}\|_F^2 v_e^T v_e + \frac{1}{4} q_e^T q_e. \end{aligned} \quad (36)$$

Submitting the control law (21), weight update law (22), and adaptive parameters (33) into (35), the

derivative of V could be rewritten as follows with incorporating (36) in the calculation:

$$\begin{aligned}
 \dot{V} &\leq -\lambda_{\min}\{\mathbf{C}\}\tilde{\boldsymbol{\eta}}^T\tilde{\boldsymbol{\eta}} - \left(\lambda_{\min}\{\mathbf{Q}\} - \sum_{m=u,v,r} \mathbf{W}_{m,ML_m} - 1\right)\tilde{\mathbf{v}}^T\tilde{\mathbf{v}} - (\lambda_{\min}\{\mathbf{k}_\eta\} - 1)\boldsymbol{\eta}_e^T\boldsymbol{\eta}_e \\
 &\quad - \sum_{m=u,v,r} \left[\left(\frac{1}{\chi_m} - \frac{1}{2} - \frac{\bar{B}_m^2}{2b}\right)q_m^2 + \left(1 - \frac{B_m^2}{\bar{B}_m^2}\right)\frac{q_m^2\bar{B}_m^2}{2b} - \frac{b}{2}\right] + \mathbf{v}_e^T \left[\mathbf{M}\dot{\boldsymbol{\beta}}_1 + \hat{\mathbf{W}}_v^T \mathbf{S}_v(\hat{\mathbf{v}})\right. \\
 &\quad - \mathbf{T}(\beta)\mathbf{g}_p \text{diag}\{\hat{\lambda}_1, \hat{\lambda}_2, \dots, \hat{\lambda}_q\}\mathbf{T}^\dagger(\beta)\boldsymbol{\alpha}_2 - \mathbf{T}(\beta)\mathbf{g}_p \text{diag}\{\tilde{\lambda}_1, \tilde{\lambda}_2, \dots, \tilde{\lambda}_q\}\mathbf{T}^\dagger(\beta)\boldsymbol{\alpha}_2 \\
 &\quad \left. + \mathbf{T}(\beta)\boldsymbol{\kappa}(\mathbf{n})\mathbf{k}_p\mathbf{A}\mathbf{B}\boldsymbol{\epsilon} - \mathbf{T}(\beta)\boldsymbol{\kappa}(\mathbf{n})\mathbf{l}(\mathbf{v}_p) + \mathbf{R}^T(\psi)\tilde{\boldsymbol{\eta}} + \mathbf{Q}\tilde{\mathbf{v}}\right] + \sum_{m=u,v,r} \tilde{\mathbf{W}}_m^T \dot{\hat{\mathbf{W}}}_m + \sum_{i=1}^q g_{pi}\tilde{\lambda}_i\dot{\lambda}_i \quad (37) \\
 &\leq -\lambda_{\min}\{\mathbf{C}\}\tilde{\boldsymbol{\eta}}^T\tilde{\boldsymbol{\eta}} - \left(\lambda_{\min}\{\mathbf{Q}\} - \sum_{m=u,v,r} \mathbf{W}_{m,ML_m} - 1\right)\tilde{\mathbf{v}}^T\tilde{\mathbf{v}} - (\lambda_{\min}\{\mathbf{k}_\eta\} - 1)\boldsymbol{\eta}_e^T\boldsymbol{\eta}_e \\
 &\quad - \sum_{m=u,v,r} \left(\frac{1}{\chi_m} - \frac{1}{2} - \frac{\bar{B}_m^2}{2b}\right)q_m^2 - \left(\lambda_{\min}\{\mathbf{k}_v\} - \|\mathbf{M} - \mathbf{I}\|_{\mathbf{F}}\chi_1^{-1}\|_{\mathbf{F}}^2 - \frac{1}{2}\right)\mathbf{v}_e^T\mathbf{v}_e \\
 &\quad - \sum_{i=1}^q \frac{\sigma_i g_{pi}}{2}\tilde{\lambda}_i^2 - \sum_{m=u,v,r} \frac{\sigma_{wm}}{2}\tilde{\mathbf{W}}_m^T\tilde{\mathbf{W}}_m + \varrho,
 \end{aligned}$$

where $\varrho = 3b/2 + \bar{\boldsymbol{\epsilon}}_v^T\bar{\boldsymbol{\epsilon}}_v + \bar{\mathbf{d}}_w^T\bar{\mathbf{d}}_w + \|\mathbf{T}(\beta)\|^2\|\bar{\boldsymbol{\kappa}}(\mathbf{n})\|^2\|\bar{\mathbf{l}}\|^2 + \|\mathbf{T}(\beta)\|^2\|\bar{\mathbf{g}}_p\|^2\|\boldsymbol{\epsilon}\|^2 + \sum_{i=1}^q(\sigma_i\bar{g}_{pi}/2)(\lambda_i - \hat{\lambda}_i(0))^2 + \sum_{m=u,v,r}(\sigma_i/2)(\mathbf{W}_m - \hat{\mathbf{W}}_m(0))^T(\mathbf{W}_m - \hat{\mathbf{W}}_m(0))$, $\bar{\mathbf{g}}_p = \text{diag}\{\bar{g}_{p1}, \bar{g}_{p2}, \dots, \bar{g}_{pq}\}$, $\bar{\mathbf{l}} = [\bar{l}_1, \bar{l}_2, \dots, \bar{l}_q]^T$ with \bar{g}_{pi} being the upper bound of g_{pi} .

Finally, Eq. (37) can be further described as

$$\dot{V} \leq -2aV + \varrho, \quad (38)$$

where $a = \{\lambda_{\min}\{\mathbf{C}\}, (\lambda_{\min}\{\mathbf{Q}\} - \sum_{m=u,v,r} \mathbf{W}_{m,ML_m} - 1), (\lambda_{\min}\{\mathbf{k}_\eta\} - 1), \sum_{m=u,v,r}(1/\chi_m - 1/2 - \bar{B}_m^2/2b), (\lambda_{\min}\{\mathbf{k}_v\} - \|\mathbf{M} - \mathbf{I}\|_{\mathbf{F}}\chi_1^{-1}\|_{\mathbf{F}}^2 - 1/2), (\sigma_1\Gamma_1/2), \dots, (\sigma_q\Gamma_q/2), (\sigma_{wu}\Gamma_{wu}/2), \dots, (\sigma_{wr}\Gamma_{wr}/2)\}$. Integrating (38), it yields $V(t) \leq \varrho/2a + (V(0) - \varrho/2a)\exp(-2at)$. Referring to the closed-loop gain shaping algorithm [30], it is concluded that all error variables $\tilde{\boldsymbol{\eta}}, \tilde{\mathbf{v}}, \boldsymbol{\eta}_e, \mathbf{v}_e, \mathbf{q}_e, \tilde{\mathbf{W}}_m, \tilde{\lambda}_i$ would fall into and remain in the attractive set $\Omega := \{(\tilde{\boldsymbol{\eta}}, \tilde{\mathbf{v}}, \boldsymbol{\eta}_e, \mathbf{v}_e, \mathbf{q}_e, \tilde{\mathbf{W}}_m, \tilde{\lambda}_i) \mid \|\tilde{\boldsymbol{\eta}}\|^2 + \|\boldsymbol{\eta}_e\|^2 + \|\mathbf{q}_e\|^2 \leq C_0, \|\tilde{\mathbf{v}}\|^2 + \|\mathbf{v}_e\|^2 \leq (C_0/\lambda_{\min}\{\mathbf{M}\}), \|\tilde{\mathbf{W}}_m\|^2 \leq (C_0/\lambda_{\min}\{\mathbf{T}_{wm}\}), \tilde{\lambda}_i^2 \leq (C_0/\Gamma_i^{-1})\}$ with $t \rightarrow \infty$, and $C_0 > \varrho/a$ is a positive constant. Therefore, the error variables $\tilde{\boldsymbol{\eta}}, \tilde{\mathbf{v}}, \boldsymbol{\eta}_e, \mathbf{v}_e, \mathbf{q}_e, \tilde{\lambda}_i, \tilde{\mathbf{W}}_m$ are all SGUUB in the closed-loop control system.

5 Numerical simulations

In this section, the numerical simulations are employed to illustrate and evaluate the effectiveness of the proposed algorithm. And the simulation results are compared with the algorithm [31] employing the hysteresis nonlinearity. Both algorithms are all designed by the fusion of the observer-based backstepping methodology, and the state variables are all estimated by the designed observer. The similar comparison can further demonstrate the effectiveness and superiority of the proposed algorithm. For this purpose, the supply marine ship (length of 76.2 m, mass of 4.591×10^6 kg) is equipped with two main propellers, one rotatable thruster and two tunnel thrusters. And the thruster configuration diagram is shown in Figure 2. The model parameters of the plant are shown in Table 1.

As to the marine environment disturbances, the sea wind and irregular wind-generated wave are simulated by the physical-based mathematical model; i.e., the NORSOK wind and the JONSWAP wave spectrums are employed to simulate these two disturbances [32, 33]. The two-dimension (2-D) wind field and the corresponding wind-generated waves with the sixth level sea state are shown in Figure 3. The wind direction $\psi_{\text{wind}} = 180^\circ$, mean wind speed $V_{\text{wind}} = 15.3$ m/s.

In this simulation, the desired attitude is $\boldsymbol{\eta}_d = [10 \text{ m}, 10 \text{ m}, 140^\circ]^T$. The initial states of the ship could be described as $[x(0), y(0), \psi(0), u(0), v(0), r(0)] = [0 \text{ m}, 0 \text{ m}, 156^\circ, 0 \text{ m/s}, 0 \text{ m/s}, 0^\circ/\text{s}]^T$ and

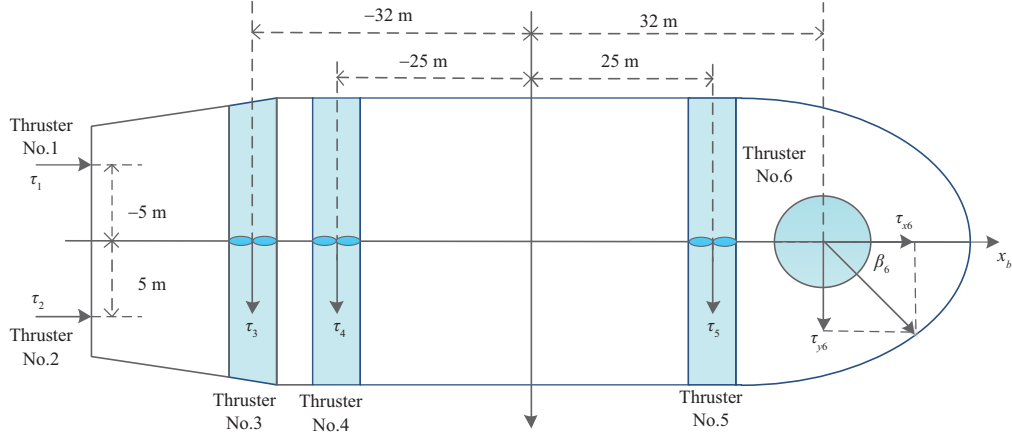
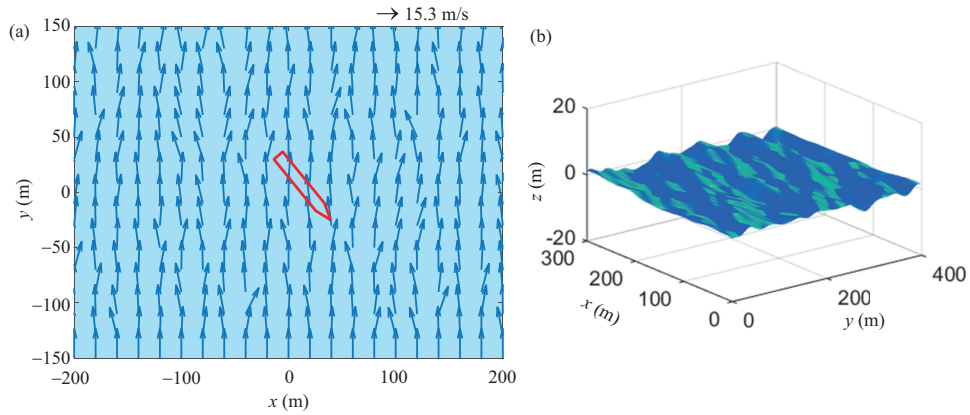

Figure 2 (Color online) Thruster configuration diagram for the supply ship ($L = 76.2$ m).

Table 1 Model parameters

Item	Value	Item	Value	Item	Value
$X_{\dot{u}}$	-0.7212×10^6	$Y_{\dot{v}}$	-3.6921×10^6	$Y_{\dot{r}}$	-1.0234×10^6
$I_z - N_{\dot{r}}$	3.7454×10^9	X_u	5.0242×10^4	Y_v	2.7229×10^5
Y_r	-4.3933×10^6	$Y_{ v v}$	1.7860×10^4	$X_{ u u}$	1.0179×10^3
$Y_{ v r}$	-3.0068×10^5	N_v	-4.3821×10^6	N_r	4.1894×10^8
$N_{ v v}$	-2.4684×10^5	$N_{ v r}$	6.5759×10^6		


Figure 3 (Color online) Marine environment disturbances. (a) 2-D wind field; (b) the corresponding wind-generated waves.

the corresponding parameters settings are given as follows with the extending operation of configuration matrix in Remark 1 being performed:

$$\begin{aligned}
 \mathbf{k}_\eta &= \text{diag}\{0.003, 0.003, 3.3\}, \quad \boldsymbol{\chi}_1 = \text{diag}\{0.01, 0.01, 0.01\}, \quad \mathbf{k}_v = \text{diag}\{0.2, 0.2, 5.5\}, \quad \mathbf{C} = \text{diag}\{5, 5, 5\}, \\
 \boldsymbol{\Gamma}_{wu} &= \boldsymbol{\Gamma}_{wv} = \boldsymbol{\Gamma}_{wr} = \text{diag}\{0.12\} \in \mathbb{R}^{25 \times 25}, \quad \sigma_{wu} = \sigma_{wv} = \sigma_{wr} = 1.7, \quad \delta_i = 1, \quad \mathbf{Q} = \text{diag}\{0.1, 0.1, 0.1\}, \\
 \boldsymbol{\Gamma} &= [0.8, 0.8, 0.2, 0.2, 0.3, 0.3, 0.2]^T, \quad \boldsymbol{\sigma} = [10.8, 10.8, 14, 12.2, 6.3, 4.2, 10.5]^T, \quad D = 0.1, \quad \epsilon_i = 0.1.
 \end{aligned} \tag{39}$$

Furthermore, the RBF NN for $\mathbf{f}_{\text{NN}}(\mathbf{v})$ contains 25 nodes with centers spaced in $[-2.5 \text{ m/s}, 2.5 \text{ m/s}]$ for the surge velocity u , $[-2.5 \text{ m/s}, 2.5 \text{ m/s}]$ for the sway velocity v , and $[-0.6 \text{ rad/s}, 0.6 \text{ rad/s}]$ for the yaw velocity r , widths $\zeta_j = 3$.

The corresponding curves of the closed-loop systems under both algorithms are given in Figures 4(a)–(c). The ship motion trajectories and the curves of ship attitude variable are shown in Figures 4(a) and (b), respectively. From Figures 4(a) and (b), it is easy to know that the steady performance under the proposed control strategy is more superior compared with the scheme [31] employing the hysteresis nonlinearity. For the quantitative purpose, one employs the following three popular performance specifications to evaluate

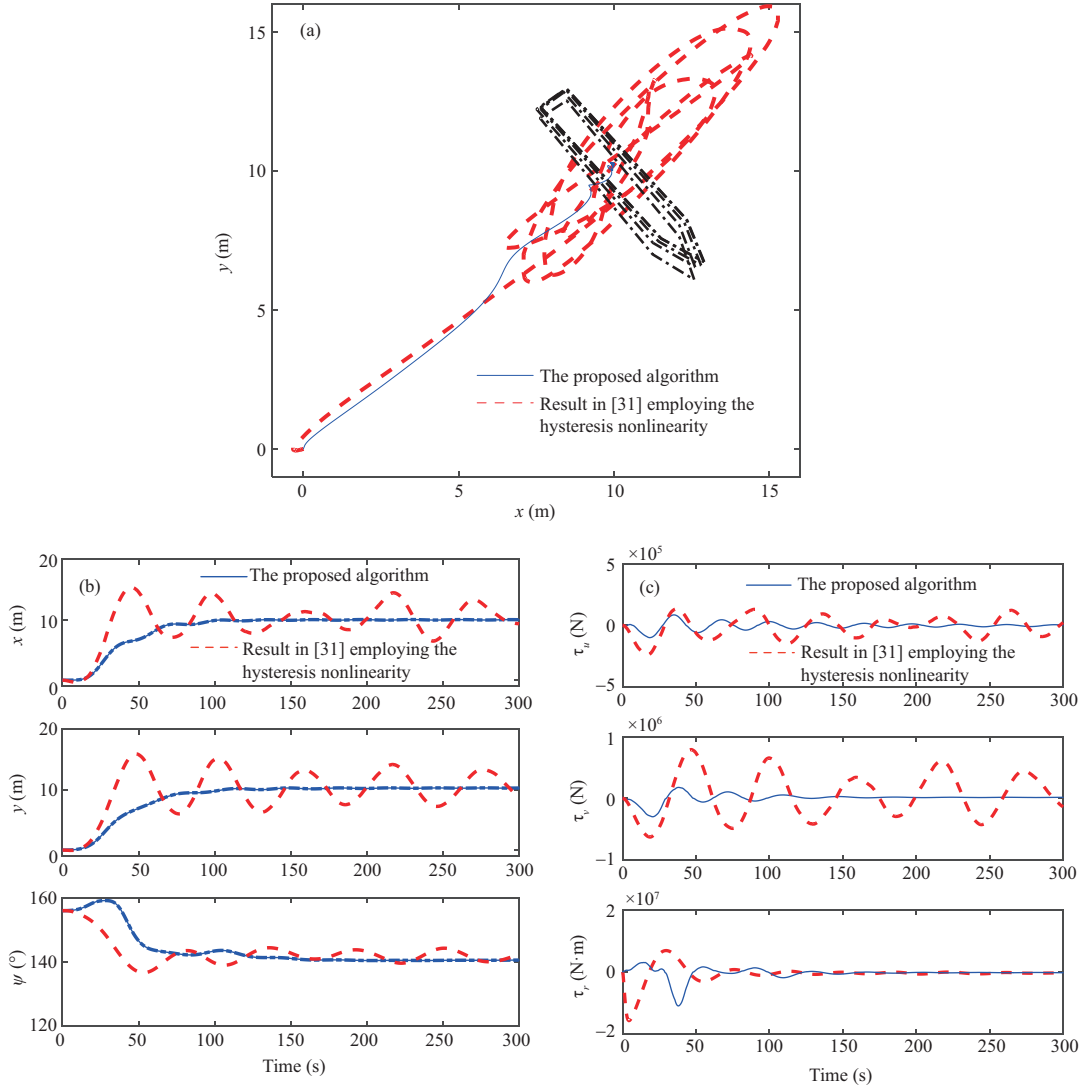


Figure 4 (Color online) (a) The ship motion trajectories; (b) the attitude variables x , y , ψ ; (c) the control efforts τ_u , τ_v and moment τ_r .

both algorithms, including the mean absolute error (MAE), the mean absolute control input (MAI), and the mean total variation (MTV) of the control input. MAE is employed to describe the performance of the system response, MAI is used to evaluate the energy consumption of the closed-loop system, and MTV is adopted to appraise the smoothness property. The corresponding quantitative comparison results are summarized as Table 2. It is easy to note that the MAE for ψ_e and MAI for τ_r are larger under the proposed algorithm than that under the algorithm [31] employing the hysteresis nonlinearity. Even so, the proposed algorithm is more reasonable in the overall view on the basis of the aforementioned indices.

Furthermore, three popular performance indices are employed to check the performance of the proposed algorithm in the aspects of communication load, i.e., triggered count (TC), maximum triggered time interval (TTI_{\max}), and minimum triggered time interval (TTI_{\min}). In these simulations, the sampling points are 3×10^4 for the conventional DP continuous-time control scheme [31] with the time increment being 0.01 s. However, as shown in Table 3, the TC is between 150 and 300 for each thruster in the proposed algorithm, which would greatly ease the communication burden. Moreover, the minimum triggered time interval reaches 1 s; i.e., there exists no Zeno behavior in this proposed algorithm. The triggered time interval between two adjacent self-triggered sampling points for thruster No.3 is shown in Figure 5. The triggered time interval figures of other thrusters are omitted due to space constraints, and the evolution of the triggered time interval for other thrusters is similar to that of thruster No.3.

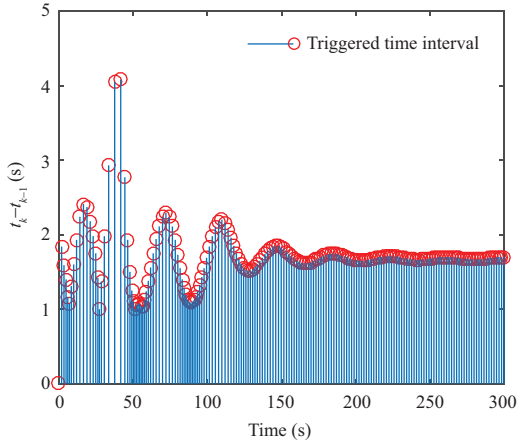
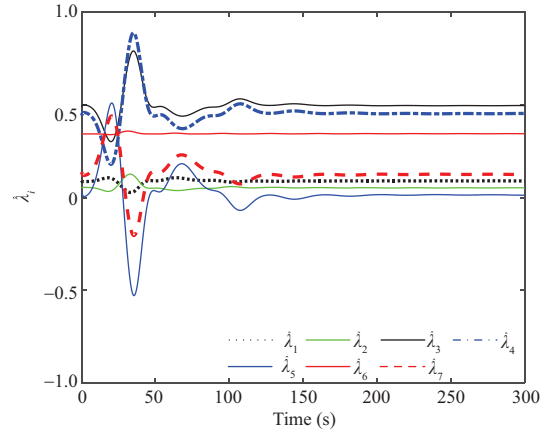
The evolution of adaptive parameters is shown in Figure 6. They are utilized to compensate for the

Table 2 Quantitative comparison of performance between the proposed algorithm and the one in [31] employing the hysteresis nonlinearity

Index	Item	The proposed algorithm	The algorithm in [31] employing the hysteresis nonlinearity
MAE	$\frac{1}{t_\infty - t_0} \int_{t_0}^{t_\infty} x_e(t) dt$ (m)	1.4060	2.5781
	$\frac{1}{t_\infty - t_0} \int_{t_0}^{t_\infty} y_e(t) dt$ (m)	1.5334	2.9893
	$\frac{1}{t_\infty - t_0} \int_{t_0}^{t_\infty} \psi_e(t) dt$ ($^\circ$)	3.8737	3.2527
MAI	$\frac{1}{t_\infty - t_0} \int_{t_0}^{t_\infty} \tau_u(t) dt$ (N)	1.8633×10^4	7.1767×10^4
	$\frac{1}{t_\infty - t_0} \int_{t_0}^{t_\infty} \tau_v(t) dt$ (N)	3.9821×10^4	3.1344×10^5
	$\frac{1}{t_\infty - t_0} \int_{t_0}^{t_\infty} \tau_r(t) dt$ (N · m)	8.6220×10^5	7.1526×10^5
MTV	$\frac{1}{t_\infty - t_0} \int_{t_0}^{t_\infty} \tau_u(t+1) - \tau_u(t) dt$ (N)	36.7429	97.0663
	$\frac{1}{t_\infty - t_0} \int_{t_0}^{t_\infty} \tau_v(t+1) - \tau_v(t) dt$ (N)	52.7663	344.2538
	$\frac{1}{t_\infty - t_0} \int_{t_0}^{t_\infty} \tau_r(t+1) - \tau_r(t) dt$ (N · m)	1435.8208	1806.7875

Table 3 Quantitative analysis for the proposed asynchronous self-triggered control scheme

	Thruster No.1	Thruster No.2	Thruster No.3	Thruster No.4	Thruster No.5	Thruster No.6 (p_6)	Thruster No.6 (β_6)
TC	269	279	178	185	272	209	252
TTI _{max} (s)	1.29	1.48	4.08	4.78	3.21	2.32	2.64
TTI _{min} (s)	1.00	1.00	1.00	1.00	1.00	1.01	1.00


Figure 5 (Color online) The triggered time interval between the two adjacent self-triggered sampling points for the thruster No.3.

Figure 6 (Color online) Adaptive parameters $\hat{\lambda}_i$ with hysteresis nonlinearity.

hysteresis nonlinearity for each thruster. To further verify the hysteresis compensation performance in this proposed control scheme, the hysteresis corresponding parameters are chosen as $\xi_i = 1$, $\zeta_i = 0.1$, $k_{pi} = 1.5$, $i = 1, 2, \dots, 7$. The curves of control inputs with hysteresis nonlinearity are shown in Figure 7. The two subplots in Figure 7 reflect the relationships among the hysteresis input, self-triggered input, and actual input for thruster No.6. The curve evolution of the hysteresis and the self-triggered inputs for thruster Nos. 1–5 is similar to thruster No.6, and they are omitted to improve the clarity and readability. The bearing angle, including that for thruster No.6 (azimuth thruster), seems to be unreasonable, but this is not the case. Actually, the action range for the bearing angle is $(-180^\circ, 180^\circ]$, and the transformation operation is required for the azimuth thruster in practical engineering. Hence, the curves of the bearing angle in Figure 7 are smooth and reasonable. The above simulation results verify the good performance of the control scheme.

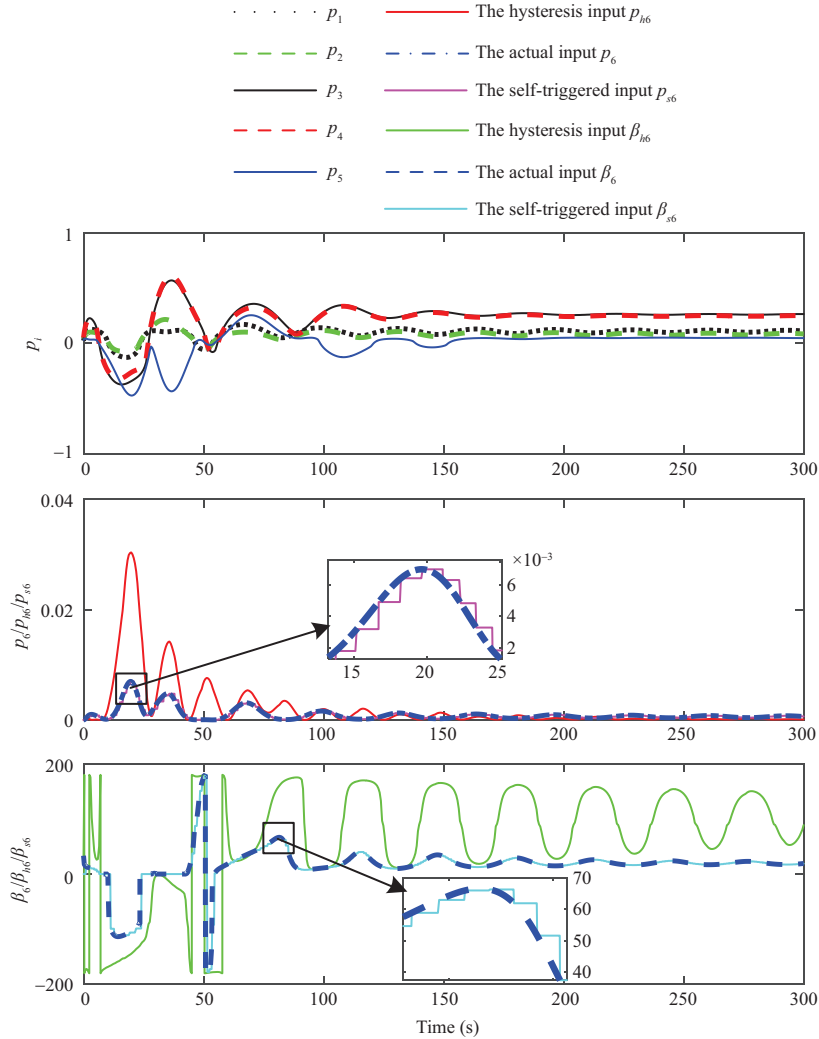


Figure 7 (Color online) Control inputs with hysteresis nonlinearity.

6 Conclusion

In this paper, we describe the development of an observer-based asynchronous self-triggered control for DP ship in the presence of the hysteresis nonlinearity. The self-triggered mechanism is designed to realize the asynchronous aperiodic transmission of control signals in controller-thruster channels, which can ease the communication burden caused by the frequent transmission of signals. Moreover, the NN observer is employed to provide the estimation of velocities including the surge, sway, and yaw velocity, and they are utilized in the controller design. Meanwhile, the unknown backlash-like hysteresis nonlinearity and gain uncertainty are simultaneously considered with the fusion of the adaptive backstepping recursive design technique. The SGUUB stability of the closed-loop control system has been demonstrated on the basis of the Lyapunov theory. The numerical simulations illustrate the performance and validity of the proposed control scheme under simulated marine environments. Aside from the DP ship, the proposed control scheme can also be extended to other marine structures (drilling rigs, offshore platforms, and FPSOs) and even general nonlinear systems.

Nonetheless, this work naturally cannot attend to every detail of the closed-loop system design, for example, nonlinear dynamics existing in thrusters, including dead-zone, saturation, and fault. This would be the problem to be solved in future work.

Acknowledgements This work was partially supported by National Natural Science Foundation of China (Grant Nos. 52171291, 51909018), Liaoning BaiQianWan Talents Program (Grant No. 2021BQWQ64), Science and Technology Innovation Foundation of Dalian City (Grant No. 2019J12GX026), Dalian Innovation Team Support Plan in the Key Research Field (Grant No. 2020RT08), and Fundamental Research Funds for the Central Universities (Grant No. 3132022128). The authors would like to thank anonymous

reviewers for their valuable comments.

References

- 1 Hassani V, Sørensen A J, Pascoal A M, et al. Robust dynamic positioning of offshore vessels using mixed- μ synthesis modeling, design, and practice. *Ocean Eng*, 2017, 129: 389–400
- 2 Hassani V, Sorensen A J, Pascoal A M, et al. Multiple model adaptive wave filtering for dynamic positioning of marine vessels. In: *Proceedings of American Control Conference (ACC)*, 2012. 6222–6228
- 3 Nguyen T D, Sørensen A J, Quek S T. Design of hybrid controller for dynamic positioning from calm to extreme sea conditions. *Automatica*, 2007, 43: 768–785
- 4 Zhang G, Yao M, Xu J, et al. Robust neural event-triggered control for dynamic positioning ships with actuator faults. *Ocean Eng*, 2020, 207: 107292
- 5 Hu X, Du J, Shi J. Adaptive fuzzy controller design for dynamic positioning system of vessels. *Appl Ocean Res*, 2015, 53: 46–53
- 6 Du J, Yang Y, Wang D, et al. A robust adaptive neural networks controller for maritime dynamic positioning system. *Neurocomputing*, 2013, 110: 128–136
- 7 Zhang G, Cai Y, Zhang W. Robust neural control for dynamic positioning ships with the optimum-seeking guidance. *IEEE Trans Syst Man Cybern Syst*, 2017, 47: 1500–1509
- 8 Xing L, Wen C, Liu Z, et al. Adaptive compensation for actuator failures with event-triggered input. *Automatica*, 2017, 85: 129–136
- 9 Xing L, Wen C, Liu Z, et al. Event-triggered adaptive control for a class of uncertain nonlinear systems. *IEEE Trans Automat Contr*, 2017, 62: 2071–2076
- 10 Sahoo A, Xu H, Jagannathan S. Neural network-based event-triggered state feedback control of nonlinear continuous-time systems. *IEEE Trans Neural Netw Learning Syst*, 2016, 27: 497–509
- 11 Hu S, Yue D, Xie X, et al. Stabilization of neural-network-based control systems via event-triggered control with nonperiodic sampled data. *IEEE Trans Neural Netw Learning Syst*, 2018, 29: 573–585
- 12 Cai J, Yu R, Yan Q, et al. Event-triggered control for strict-feedback nonlinear systems with external disturbances. *IEEE Access*, 2019, 7: 38390–38396
- 13 Huang J, Wang W, Wen C, et al. Adaptive event-triggered control of nonlinear systems with controller and parameter estimator triggering. *IEEE Trans Automat Contr*, 2020, 65: 318–324
- 14 Sun J, Yang J, Li S, et al. Estimate-based dynamic event-triggered output feedback control of networked nonlinear uncertain systems. *IEEE Trans Syst Man Cybern Syst*, 2021, 51: 3148–3158
- 15 Du J, Hu X, Liu H, et al. Adaptive robust output feedback control for a marine dynamic positioning system based on a high-gain observer. *IEEE Trans Neural Netw Learning Syst*, 2015, 26: 2775–2786
- 16 Yi B, Wang R, Manchester I R. Reduced-order nonlinear observers via contraction analysis and convex optimization. *IEEE Trans Automat Contr*, 2022, 67: 4045–4060
- 17 Gao Y, Sun G, Liu J, et al. State estimation and self-triggered control of CPSs against joint sensor and actuator attacks. *Automatica*, 2020, 113: 108687
- 18 Mazo J M, Anta A, Tabuada P. An ISS self-triggered implementation of linear controllers. *Automatica*, 2010, 46: 1310–1314
- 19 Brunner F D, Heemels M, Allgöwer F. Robust self-triggered MPC for constrained linear systems: a tube-based approach. *Automatica*, 2016, 72: 73–83
- 20 Shen F, Wang X, Yin X. BLF-based adaptive DSC for a class of stochastic nonlinear systems of full state constraints with time delay and hysteresis input. *Neurocomputing*, 2020, 386: 244–256
- 21 Lin X, Nie J, Jiao Y, et al. Nonlinear adaptive fuzzy output-feedback controller design for dynamic positioning system of ships. *Ocean Eng*, 2018, 158: 186–195
- 22 Pan Y, Zhou Y, Sun T, et al. Composite adaptive fuzzy H_∞ tracking control of uncertain nonlinear systems. *Neurocomputing*, 2013, 99: 15–24
- 23 Xu B, Shi Z, Yang C, et al. Composite neural dynamic surface control of a class of uncertain nonlinear systems in strict-feedback form. *IEEE Trans Cybern*, 2014, 44: 2626–2634
- 24 Fossen T I, Strand J P. Nonlinear passive weather optimal positioning control (WOPC) system for ships and rigs: experimental results. *Automatica*, 2001, 37: 701–715
- 25 Su C Y, Stepanenko Y, Svoboda J, et al. Robust adaptive control of a class of nonlinear systems with unknown backlash-like hysteresis. *IEEE Trans Automat Contr*, 2000, 45: 2427–2432
- 26 Zhang G, Li J, Jin X, et al. Robust adaptive neural control for wing-sail-assisted vehicle via the multiport event-triggered approach. *IEEE Trans Cybern*, 2021. doi: 10.1109/TCYB.2021.3091580
- 27 Chen B, Liu X, Liu K, et al. Novel adaptive neural control design for nonlinear MIMO time-delay systems. *Automatica*, 2009, 45: 1554–1560
- 28 Li Y X, Yang G H. Model-based adaptive event-triggered control of strict-feedback nonlinear systems. *IEEE Trans Neural Netw Learning Syst*, 2018, 29: 1033–1045
- 29 Li Y X, Yang G H. Event-triggered adaptive backstepping control for parametric strict-feedback nonlinear systems. *Int J Robust Nonlinear Control*, 2018, 28: 976–1000
- 30 Li J, Zhang G, Liu C, et al. COLREGs-constrained adaptive fuzzy event-triggered control for underactuated surface vessels with the actuator failures. *IEEE Trans Fuzzy Syst*, 2021, 29: 3822–3832
- 31 Morishita H M, Souza C E S. Modified observer backstepping controller for a dynamic positioning system. *Control Eng Practice*, 2014, 33: 105–114
- 32 Fossen T I. *Handbook of Marine Craft Hydrodynamics and Motion Control*. New York: Wiley, 2011
- 33 Li J, Zhang G, Li B. Robust adaptive neural cooperative control for the USV-UAV based on the LVS-LVA guidance principle. *J Marine Sci Eng*, 2022, 10: 51